Nanoscale ordering and multiferroic behavior in $Pb(Fe_{1/2}Ta_{1/2})O_3$

R. Martinez,[1] R. Palai,[1,*] H. Huhtinen,[2] J. Liu,[3] J. F. Scott,[4] and R. S. Katiyar[1]
[1]*Department of Physics and Institute for Functional Nanomaterials, University of Puerto Rico, San Juan, Puerto Rico 00931, USA*
[2]*Wihuri Physical Laboratory, Department of Physics and Astronomy, University of Turku, Turku FIN-20014, Finland*
[3]*Rensselaer Polytechnic Institute, Center for Terahertz Research, 110 8th Street, Troy, New York 12180, USA*
[4]*Department of Physics, Cavendish Laboratory, University of Cambridge, Cambridge CB3 0HE, United Kingdom*
(Received 11 May 2010; revised manuscript received 2 September 2010; published 5 October 2010; publisher error corrected 8 October 2010)

We report on structural, microstructural, dielectric, electrical, magnetic, and spectroscopic (Raman and terahertz) properties of lead iron tantalate $Pb(Fe_{1/2}Ta_{1/2})O_3$ ceramics. Raman spectroscopy revealed the presence of nanoscale ordering though it is forbidden in bulk by crystal symmetry. The dielectric properties of $Pb(Fe_{1/2}Ta_{1/2})O_3$ show a typical relaxor ferroelectric behavior with long-range disorder while the magnetoelectric properties show an interesting multiferroic behavior (coexistence of ferroelectric and magnetic order) in the same phase. The temperature variation in field cooled magnetization shows anomalies at about 55($\pm$5) and 180($\pm$5) K indicating the existence of two Néel temperatures in agreement with theoretical predictions. The zero-field-cooled magnetization as a function temperature and field reveals the existence of spin-glasslike behavior at low temperature like single crystal. The electrical conduction behavior satisfies the modified Schottky equation of Simmons at all fields. The ac conductivity as a function of frequency shows an excellent fit to the universal power law. Terahertz spectroscopy shows an opaque nature of $Pb(Fe_{1/2}Ta_{1/2})O_3$ in midinfrared and far-infrared wavelengths.

DOI: 10.1103/PhysRevB.82.134104 PACS number(s): 75.85.+t, 91.25.F−, 61.66.Bi, 77.80.Jk

I. INTRODUCTION

$Pb(Fe_{1/2}Ta_{1/2})O_3$ (PFT) is a relaxor ferroelectric with Curie temperature (T_c) slightly below ambient temperature.[1] The crystallographic properties of single crystal PFT have extensively been studied both experimentally using x-ray diffraction (XRD) and polarized light microscopy[1–7] and neutron diffraction,[8] and theoretically[9] using first-principles density-functional theory (DFT) and Vienna *ab initio* simulation package (VASP). Recent reports show that PFT possesses an ideal cubic ($Pm\bar{3}m$) phase ($T>T_{c1}=270$ K), a tetragonal ($P4mm$) intermediate phase (270 K$>T>$220 K), and a low-temperature monoclinic (Cm) structure ($T<T_{c2}=220$ K);[8] contrary to the earlier report cubic ($Pm\bar{3}m$), $T>T_{c1}=248$ K$\rightarrow$monoclinic, 248 K$>T>$210 K$\rightarrow$rhombohedral ($R3m$), $T<210$ K.[1–5] However, still many uncertainties remain, e.g., Brixel *et al.*,[4] and Geddo Lehmann *et al.*,[5] reported the observation of optical anisotropy and uniaxial birefringence in an *as-grown* PFT single crystal in the paraelectric cubic phase. In fact the existence of a weak uniaxial birefringence indicates a tetragonal symmetry.[5] A uniaxial optical anisotropy was reported in cubic boracites[10–12] and uniaxial birefringence was observed in $BaTiO_3$, above T_c (Ref. 13) and in cubic $SrTiO_3$ (Ref. 14) because of the deformed surface layer due to mechanical polishing but the stress effect was eliminated or reduced by thermal annealing and chemical etching.[13,14] However, the observation of reproducible uniaxial birefringence and optical anisotropy by Geddo Lehmann *et al.*[5] in as-grown cubic PFT at room temperature (RT) is unexplained, and the critical question, *"Is there a hidden symmetry breaking?"* raised by them still remains unanswered, which warrants further investigation.

PFT is one of the first-known perovskites in which magnetic Fe^{3+} ($3d^5$, $S=5/2$) and a nonmagnetic Ta^{5+} ($3d^0$, $S=0$) ions share the B site of the simple perovskite structure. The compound shows simultaneous magnetic and electric (multiferroic) ordering in the same phase. The physics of such materials is strongly influenced by the underlying chemical distribution of B cations in the octahedral sublattice of the perovskite structure, and in this compound both the Fe^{3+} and Ta^{5+} cations are randomly distributed on octahedral sites. There are a few reports[2,15] on magnetic and magnetoelectric properties of single crystals but no detailed study has been done on magnetoelectric properties of PFT in polycrystalline or in thin film form.

The motivation for the present study is manifold. One of the objectives is to use micro-Raman spectroscopy to explore the structural complexity of PFT, and others are to understand the magnetic, dielectric, electrical, magnetoelectric, and terahertz (THz) properties of polycrystalline PFT.

II. EXPERIMENTAL DETAILS

Polycrystalline samples of PFT were prepared using high purity PbO, Fe_2O_3, and Ta_2O_5 as starting materials. The powders of materials were mixed in stoichiometric ratio with 10 wt % excess of PbO to compensate Pb deficiency during the high-temperature processing, followed by high-energy ball milling, using tungsten balls in a methanol medium for 16 h. The mixture was calcined in air at 950 °C in covered crucibles with intermediate grinding and ball milling for 5 h, and finally, pressed into pellets of 7.25 mm diameter and 1.24 mm thick, under a pressure of 3530 kg/cm^2. The pellets were sintered at 1050 °C in an alumina crucible for 15 h with heating and cooling rates of 10 °C/min. Details of synthesis and characterization of PFT by sol-gel and solid-state routs are given in.[16] Structural properties of the samples were carried out by using a Siemens D5000 x-ray diffractometer

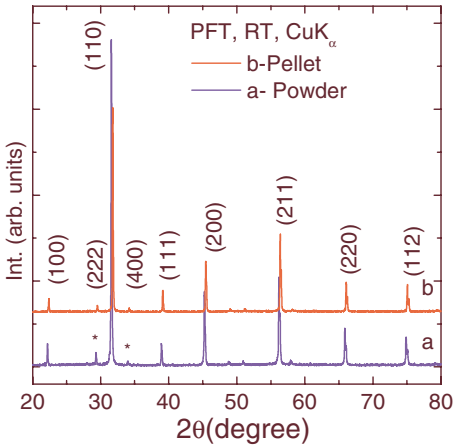

FIG. 1. (Color online) XRD pattern of $Pb(Fe_{1/2}Ta_{1/2})O_3$ at room temperature; (a) powders calcined at 950 °C; (b) Pellets sintered at 1050 °C. The presence of pyrochlore phase is indicated with "*" marks.

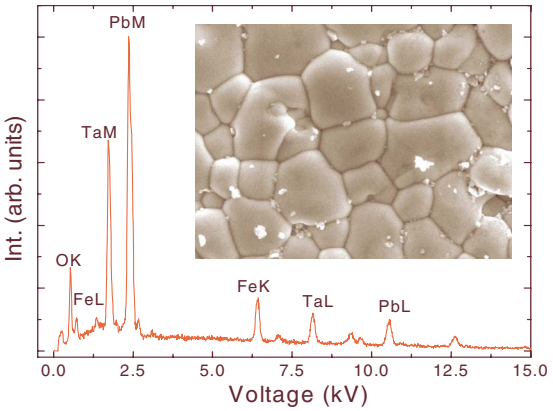

FIG. 2. (Color online) EDS spectrum of $Pb(Fe_{1/2}Ta_{1/2})O_3$ at room temperature (295 K). The inset shows SEM micrograph of fractured surface of the pellet.

using Cu $K\alpha$ ($\lambda = 1.5406$ Å) radiation. For the dielectric and electrical measurements the pellets were polished and sputtered with platinum electrodes. Dielectric and electrical polarization (hysteresis) measurements were conducted using impedance analyzers (model MMR K-20, HP4294A, and HIOKI 3532–50 LCR Hister) and radiant technology loop tester. The dielectric permittivity was measured at different frequencies (42–5 MHz) and temperatures (77–380 K). The micro-Raman measurements were performed in the backscattering geometry using the Jobin-Yvon T64000 spectrometer. Excitation radiation of 514.5 nm from a coherent argon ion laser was focused to ~2 μm^2 on the sample surface. The magnetic measurement was performed using a vibrating sample magnetometer (VSM Lakeshore model 142A) and superconducting quantum interference devices magnetometers from 4–300 K. A THz time domain spectroscopy system was used to measure the transmission spectra in the range of 0.1–3.0 THz and a Fourier transform infrared (FTIR) system used to measure the transmission spectroscopy in the range of 0.1–22 THz.

III. RESULTS AND DISCUSSION

A. Structural and microstructural properties

The XRD pattern (Fig. 1) of PFT ceramic powder and pellet taken at RT confirms the formation of a single-phase perovskite structure. However, a very small amount of pyrochlore phase (marked with *star* on the XRD pattern) was detected in powder samples and was insignificantly small in the pellet after sintering at 1050 °C. The percentage of perovskite phase was calculated using the standard formula[17] and was found to be 96.54% in powder sample and almost 97.3% in pellet. The exact composition of the pyrochlore phase in our samples is not known. However, the common pyrochlore phases associated with Pb and Ta are $Pb_2Ta_2O_7$, $Pb_3Ta_2O_8$, and $Pb_3Ta_4O_{13}$. Almost all the pyrochlore phases are dielectric (nonferroelectric) and diamagnetic [or paramagnetic (PM)]. The presence of a pyrochlore phase could reduce the dielectric permittivity due to the series effect of capacitors. It also contributes to the reduction in electrical polarization and prevents the polarization to saturate. Depending on the strength of the diamagnetic signal, the pyrochlore phase has also similar effect on magnetization. The saturation of magnetization also can be affected by the presence of linear paramagnetic behavior.

The XRD pattern was analyzed with different crystal classes using a program package[18] and the cubic structure with $a = 4.005(\pm 0.002)$ Å was selected for which standard deviation was found to be minimum, which agrees well with the reported results.[1–5] In order to study the chemical composition, energy dispersive x-ray spectroscopy (EDS) was carried out on the pellet. The EDS spectrum (Fig. 2) of the sample shows the presence of all the elements. The scanning electron microscopy (SEM) micrograph for pellet (inset Fig. 2) taken on a fractured surface of PFT pellet shows uniform distribution of grains of an average grain size of ~3 μm throughout the surface of the sample.

B. Micro-Raman spectroscopy

The PFT has an ideal cubic crystal structure above 270 K (Ref. 8) (248 K according to earlier reports[1–7]) with $Pm\bar{3}m$ space group, for which any first-order Raman actives modes are forbidden. Figure 3(a) shows the Raman spectra of PFT from 82–300 K. As can be seen, the Raman spectrum of PFT at RT shows peaks at around 135, 200, 272, 432, 695, and 854 cm^{-1}, which indicates the evidence of symmetry breaking in the cubic structures. This could be due to the presence of nanoscale ordering (polar nanoregions), which cannot be detected with x-ray diffraction. The presence of a short-range ordering was inferred by Nomura *et al.*[2] The order or disorder state of a perovskite is mostly determined from the charge difference and difference in ionic radius of the ions at the *B* site. The ionic radii of Fe^{3+} (0.64 Å) and Ta^{5+} (0.64 Å) are equal for octahedral (for equal coordination number) structure.[19] A substitution of Fe^{3+} and Ta^{5+} could produce a disorder distribution. However, on the other hand the Madelung energy due to charge ordering for a perovskite compound with cubic structure is very high

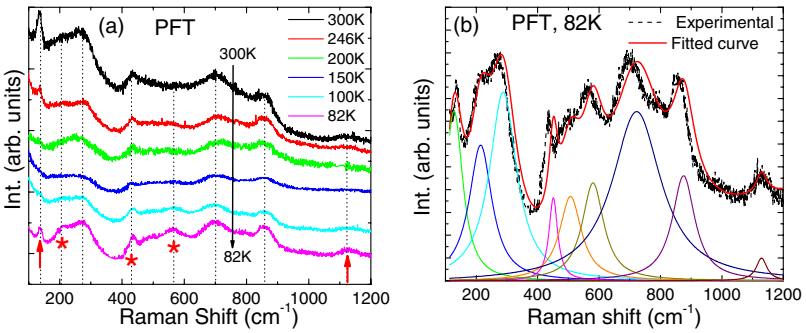

FIG. 3. (Color online) Raman spectra of $Pb(Fe_{1/2}Ta_{1/2})O_3$; (a) temperature dependent from 82 to 300 K; (b) deconvolution of the spectrum at 82 K showing evolution of peaks at 132, 212, 281, 434, 490, 562, 709, 889, and 1124 cm^{-1} and fitting (red solid line) after the deconvolution. Dotted lines, arrows, and stars are given in (a) to guide to the eyes.

(140 Kcal mol^{-1}) compared to the increase in entropy due to the disordering (1.37 Kcal mol^{-1}).[20] This should favor a more stable ordered state subject to no influence from other effects. Since the oxygen ion has large electronic polarizability it might reduce the electrostatic energy, which may favor a short-range ordered distribution.[2]

The deconvolution of the spectrum at 82 K [Fig. 3(b)] shows peaks at 132, 212, 281, 434, 490, 562, 709, 889, and 1124 cm^{-1}. A closer and careful observation reveals two characteristic features: the peaks at 212, 443, and 562 cm^{-1} [marked with stars in Fig. 3(a)] lose intensity with gradually increasing temperature and completely disappeared at 200 K; the peaks 132 and 1124 cm^{-1} [marked with "arrows" in Fig. 3(a)] lose intensity with increasing temperature and reappeared at 246 K and then show increase in intensity with increasing temperature. These phonon anomalies imply an occurrence of a structural phase transition, monoclinic to tetragonal at 200 K and tetragonal to cubic at 246 K. The observed transition temperatures agree with reported results.[1–7]

C. Magnetodielectric coupling

Figure 4 shows the frequency variation in real part of dielectric permittivity (ε') and dielectric loss tangent (tan δ) of PFT at 295 and 77 K at different applied magnetic fields. As can be seen from Fig. 4(a), a dielectric resonance has been observed at around 1.5 MHz at 295 K. Shifting of about 0.2 MHz in resonance frequency was observed between zero field and 0.023 T and then almost no difference between 0.023 and 0.55 T. Above 0.55 T a gradual shifting was observed with increasing magnetic field. The relatively larger shifting (0.2 MHz) between zero field and 0.023 T is not very clear. Magnetodielectric measurements were carried out using a special probe, different than low-temperature and high-temperature probes. This could be one of the causes of the relatively larger shifting. Since both the shifting in resonance frequency and the reduction in intensity have been observed, this could be an intrinsic effect because of the magnetic field due to the high inductance of the PFT capacitor.

The shifting of the resonance peak to higher frequencies is possibly due to the increasing the stiffness of the system with increasing magnetic field. The resonance was shifted to 4.0 MHz at 77 K. This also can be explained in terms of increasing stiffness of the system due to suppression of thermal energy. The exact nature of resonance is not very clear yet, however, it could be due to the orientation of polarization.[21,22] Note that this resonance is not just arise as an *RC*-time constant with zero inductance but an actual inductance with a phase lag. The observed resonance is very similar to the typical resonance observed in series *LCR* equivalent circuit.[23] The frequency variation in tan δ [Fig. 4(b)] shows a peak at resonance frequency (ω_0), and the shifting of the peak toward higher frequencies has also been observed with applied magnetic field. The dielectric loss is quite low except at around ω_0, which could be useful for high-frequency applications.

Figure 5(a) shows the frequency variation in impedance (Z) of PFT at 295 K with different applied magnetic fields.

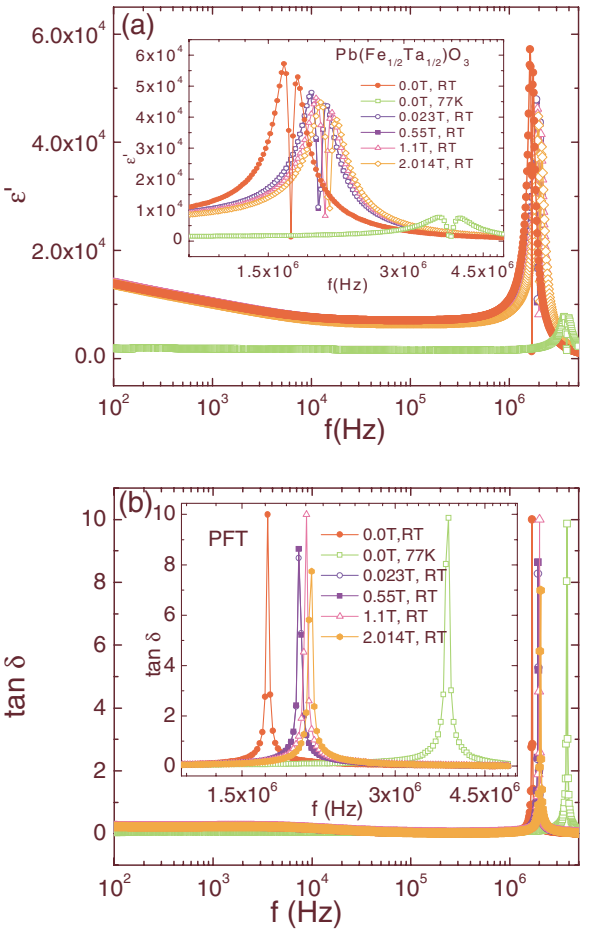

FIG. 4. (Color online) Magnetodielectric properties of $Pb(Fe_{1/2}Ta_{1/2})O_3$. Frequency variation in (a) ε' and (b) tan δ at room temperature (295 K) and 77 K and at different applied magnetic fields.

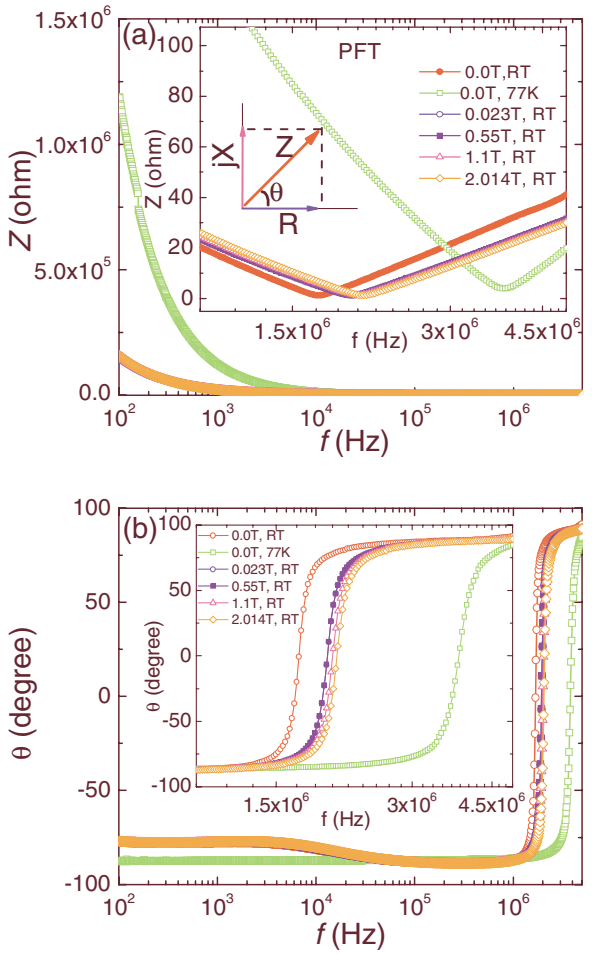

FIG. 5. (Color online) Frequency variation in (a) impedance (Z) and (b) phase angle (θ) of $Pb(Fe_{1/2}Ta_{1/2})O_3$ at different temperatures and magnetic fields. The inset in (a) shows the representation of phase angle (θ) between resistance R (real part) and reactance X (imaginary part).

As can be seen, a dip has been observed at ω_0, and it shifts toward higher frequencies with increasing magnetic field. A small increase in impedance was observed up to ω_0 with increasing magnetic field while a reverse effect was seen above ω_0. The high impedance observed at 77 K below ω_0 compared to 295 K values is a typical behavior of dielectrics whereas it is low above ω_0.

Figure 5(b) shows the frequency variation in phase angle θ [the angle between real and imaginary part of impedance, see inset Fig. 5(a)] in PFT at 295 K with different magnetic fields. This provides some interesting information about phase change. At the resonance frequency it shows a change in phase angle from −90° to +90°, indicating a change in behavior from pure capacitive to pure inductive type. A phase change in 180° is predicted at resonance in dielectrics at high frequencies.[24] The resonance frequency (the frequency at which the phase angle changes) shifts toward the higher frequencies with increasing magnetic field and at low temperature (77 K).

The origin of the inductive behavior in $Pb(Fe_{1/2}Ta_{1/2})O_3$ capacitor is not yet well understood. In general, the impedance of a capacitor decreases with frequency while that of an inductor increases. We observed a typical capacitive behavior up to 1.5 MHz. The inductive behavior which appears in the high-frequency range is usually caused by the inductance of the connecting wires, or by the inductance of the electrode, or by instrumental artifacts. We have tested samples with Ag and Au electrodes and the observation of the exactly similar effects rules out the effect of electrodes. Before doing the capacitance measurements, we calibrated the equipment with "short circuit" and "open circuit" compensations. So, the parasitic inductance from the connecting wires could not be so high as observed. Low inductance has been observed in some Ta capacitors.[25] We believe that the observed high inductance could be intrinsic in nature and might be related to the presence of Ta. The other possible effects that might have contributed to the observed high inductance may be the constant phase element effects caused by the inhomogeneities in the sample or the presence of bulk strain effect produced by the polarization gradient. Capacitors with small internal inductance are very useful for the power distribution networks for microprocessors. In the case of energy storage capacitors with small internal inductance tend to delay the discharge energy.[25]

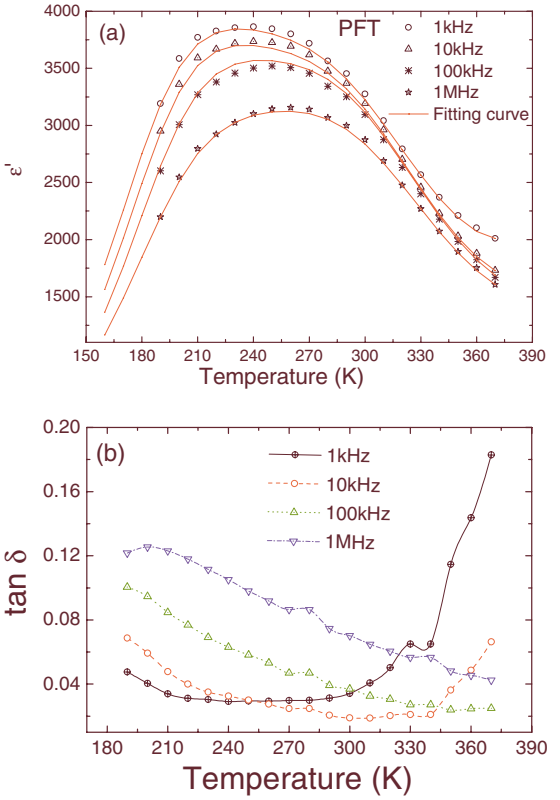

FIG. 6. (Color online) Temperature variation in (a) dielectric permittivity, ε' and (b) dielectric loss, tan δ of $Pb(Fe_{1/2}Ta_{1/2})O_3$.

D. Dielectric and electrical properties

Figure 6(a) shows the temperature (T) variation in ε' of PFT at different frequencies. The ε' shows a diffuse ferroelectric phase transition and maximum dielectric permittivity of 3870 at 240 K and 1 kHz, in agreement with reported

results[2,26,27] but this is relatively low compared to the high value (17 000 at 1 kHz) reported in.[17] The reported high value in[17] could be an extrinsic effect, e.g., space charge polarization effect. The temperature dependence of ε' vs T of PFT does not follow the Curie-Weiss law but it can be described by the following behavior,[2] this behavior is *not* a breakdown of the usual mean-field theory and its associated exponents but merely a well-known signature of relaxor dynamics:

$$\frac{1}{\varepsilon'} = A + B(T - T_m)^{\gamma}, \tag{1}$$

where A, B, T_m (temperature corresponding to the maximum ε'), and γ are variable parameters. In Fig. 6(a), the *solid line* represents the fitting of Eq. (1) to the experimental data. The value of fitted parameters obtained using Eq. (1) at 1 kHz was $A=2.6\times10^{-4}$, $B=1.2\times10^{-8}$, and critical exponent $\gamma=2$, which indicates relaxor character, with estimated maximum permittivity of 3850. The ε' vs T at different frequencies shows a diffuse phase transition and frequency relaxation, which is a typical behavior of relaxor ferroelectrics.[2,26,27] Figure 6(b) shows the temperature variation in tan δ of PFT at different frequencies. As can be seen, at low temperature (<270 K) the loss increases with frequency while it decreases with frequency at high temperatures, except for 1 MHz, which shows slightly higher loss than 100 kHz. An anomaly in the loss has been seen at around 280 and 345 K.

The current-voltage (I-V) characteristic [Fig. 7(a)] of PFT at room temperature shows a non-Ohmic behavior. The conduction behavior follows the metal-insulator-metal capacitor behavior described by modified Simmons model,[28] which is widely used to explain the conduction mechanism in oxide tunnel barriers. The model is based on only three important parameters: the barrier height (φ_0) in V, the shape factor (ρ) in V^{-1}, and the equilibrium conductance (G_0) in Ω^{-1}. The current (I) can be represented as,

$$I = \frac{2G_0\varphi_0}{\rho\varphi_0 - 2}\left\{\left(1 - \frac{V}{2\varphi_0}\right)\exp\left[\rho\varphi_0\left(1 - \sqrt{1 - \frac{V}{2\varphi_0}}\right)\right] - \left(1 + \frac{V}{2\varphi_0}\right)\exp\left[\rho\varphi_0\left(1 - \sqrt{1 + \frac{V}{2\varphi_0}}\right)\right]\right\}. \tag{2}$$

In Fig. 7(a), the solid line represents the fitting of Eq. (2) to the experimental data. As can be seen, the data show excellent fitting to Eq. (2). The value of the fitted parameters obtained using Eq. (2) was $G_0=8.2\times10^{-9}$ Ω^{-1}, $\varphi_0=-8.6\times10^{-2}$ V, and $\rho=6.6\times10^{-1}$ V^{-1}.

Figure 7(b) shows the ac conductivity (σ_{ac}) of the PFT obtained from the dielectric measurements using the formula $\sigma=\sigma_0\omega\epsilon_0\epsilon$ tan δ, where ω is angular frequency, ϵ_0 is vacuum dielectric permittivity. Generally, σ_{ac} of dielectrics increases with increasing both the frequency and the temperature. It is interesting to note here that the conductivity is decreasing with increasing temperature at higher frequencies (>100 kHz). The conductivity at 1 and 10 kHz decreases with increasing temperature up to 270 K and 340 K, respectively, and then slowly increases with increasing temperature. As can be seen from Fig. 7(b), the conductivity vary strongly with frequency. Since all the ferroelectric hysteresis measurements were carried out at 60 Hz it is believed that the sample was in good resistive state. The activation energy E_a was calculated using the following relation:

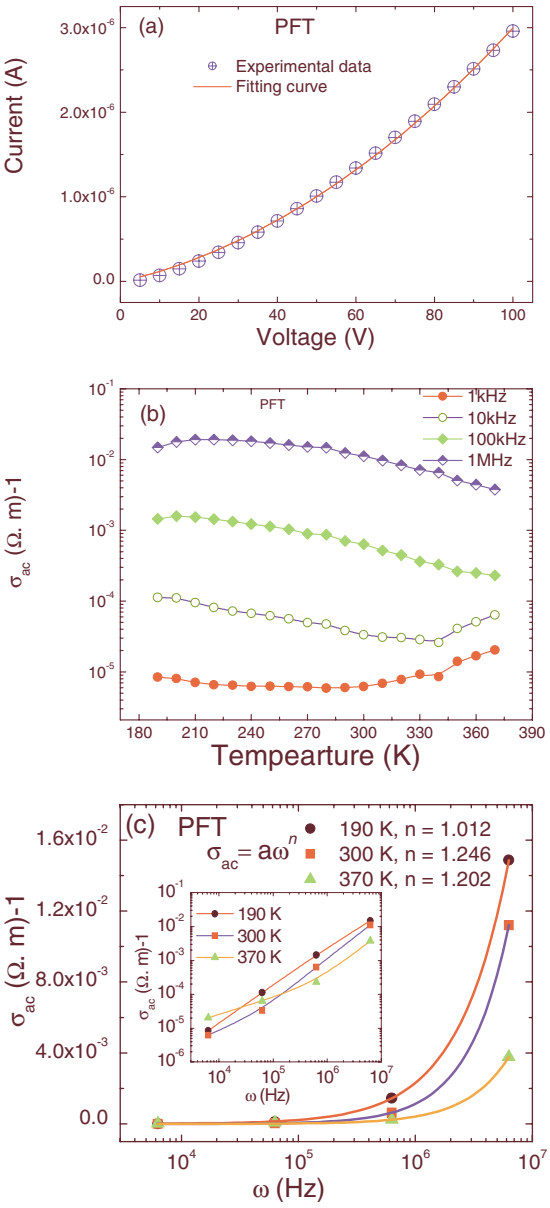

FIG. 7. (Color online) Current-Voltage (I-V) characteristic at (a) RT and (b) ac conductivity (σ_{ac}) as function of temperature, and (c) frequency of $Pb(Fe_{1/2}Ta_{1/2})O_3$. The solid line in (a) and (c) is fitted to the data using Eq. (2) and Eq. (4), respectively. Inset shows the log-log plot of ac conductivity and frequency to show better fit on all the scales.

$$\sigma_{ac} = \sigma_0 e^{(-E_a/kT)}, \tag{3}$$

where k is the Boltzmann constant and σ_0 a pre-exponential factor and found to be 0.31 eV below 50 kHz and 0.13 eV above. This low activation energy implies the existence of extrinsic conduction mechanism. In the case of the intrinsic band conduction the activation energy is usually half the

bandgap.[29] The exact nature of conduction mechanism in ceramics is very complex and far from fully understood. Probably it involves both the ionic and electronic charge carriers, and the balance depends upon temperature and ambient atmosphere. The presence of impurity atoms, oxygen vacancy, grain boundary, space charge, etc., can contribute to the conduction mechanism. In compounds containing transition metal ions, such as PFT, hopping could arise due to the electron transfer between the ions of the same element in different oxidation states.

From Fig. 7(b) it was observed that the ac conductivity (σ_{ac}) increases with increasing frequency. Figure 7(c) shows the ac conductivity of PFT as function of frequency (f) at different constant temperatures (190, 300, and 370 K). The ac conductivity versus frequency plots were analyzed by universal power law[30,31]

$$\sigma_{ac} = A\omega^n, \tag{4}$$

where A is the pre-exponential factor and the value of the exponent n evidences for the type of the dominant conductivity mechanism and concentration of mobile carriers in the material. This power law is related to the dynamics of the ionic hopping transport between localized sites. The exponent n is the measure of the degree of interaction with the environment. The exponent in the range of 0.6–1.0 indicates more disordered (amorphous) system and the conduction is mostly associated with diffusion limited hopping. Exponent $n \approx 1$ implies ideal long-range (band-to-band) conduction, which is normally observed at low temperature whereas $n > 1$ indicates the presence of thermally activated hopping process between two sites separated by energy barrier. As can be seen, the data show an excellent fit (solid line) to the universal power law [Eq. (4)]. Inset in Fig. 7(c) shows the log-log plot of ac conductivity and frequency of PFT to show better fit on all the scales. At low frequencies (<100 kHz) the conductivity is almost constant and independent of temperature. This could be related to dc conduction. The value of A was calculated from the fitting and was found to be 1.942×10^{-9}, 3.767×10^{-11}, and 2.512×10^{-11} at 190 K, 300 K, and 370 K, respectively. The value of n was found be 1.012(±0.006), 1.246(±0.002), and 1.202(±0.006) at 190 K, 300 K, and 370 K, respectively. This shows that PFT has an ideal long-range pathway conduction process at 190 K whereas it has a thermally activated hopping-type conduction process above room temperature (≥300 K).

E. Ferroelectric properties

Figure 8 shows the ferroelectric hysteresis loop of PFT at different temperatures and drive voltages at 60 Hz. A well-defined hysteresis loop [Fig. 8(a)] has been observed at 200 K with drive voltage of ±500 V. The loop [Fig. 8(b)] at 225 K with different drive voltage shows a typical relaxor ferroelectric behavior. However, it did not achieve the saturation of polarization. This is because it is close to the paraelectric phase or the applied field is not adequate at 225 K. The loop at room temperature (in the paraelectric phase) still shows a *ferroelectriclike* behavior with the maximum polarization (P_m) of ~1.4 $\mu C/cm^2$ and remnant polarization (P_r) of

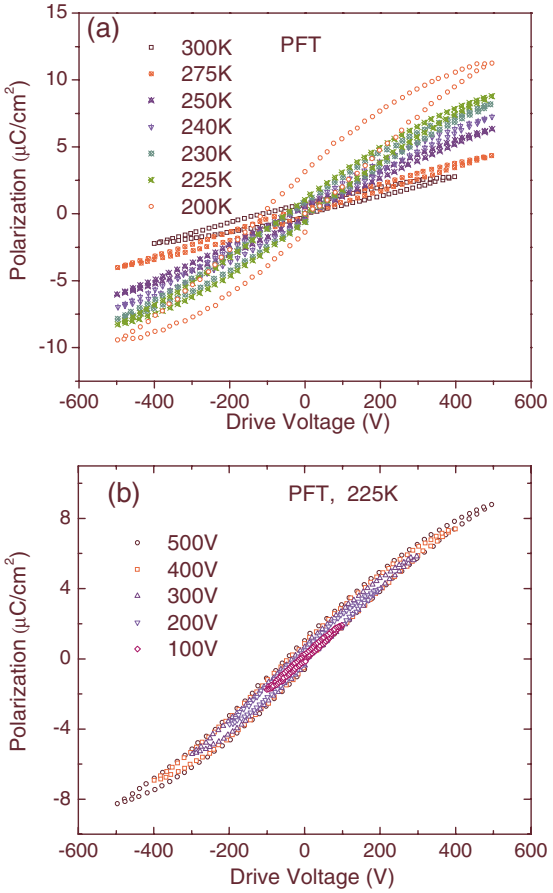

FIG. 8. (Color online) Ferroelectric hysteresis loop of $Pb(Fe_{1/2}Ta_{1/2})O_3$ at (a) different temperatures and (b) drive voltages at 225 K.

~0.25 $\mu C/cm^2$. This behavior cannot be due to the leakage effect as PFT has very low dielectric loss at room temperature. This is rather unusual for a compound which has the ferroelectric phase transition at 248 K. This implies that the compound has broken symmetry possibly due to presence of nanoscale ordering, which agrees with the observation of some forbidden Raman active modes at room temperature. The possible explanation of short-range ordering in PFT is given in Sec. III B. The presence of disordered distribution of the ions at the B site of PFT might have caused the stress in the crystal, leading to a broad ferroelectric transition, which agrees with our dielectric and electric measurements.

F. Magnetic properties

Figure 9 shows the M-H loop of PFT showing hysteresis behavior between M vs H at room temperature. A well-defined magnetic hysteresis loop of PFT at room temperature shows the presence of magnetic ordering. The exact nature of magnetic ordering is not clear yet. In order to understand the nature of magnetic ordering, temperature variation in magnetization (M) has been investigated at different applied magnetic fields.

Figure 10 shows the temperature dependence of field cooled (FC) and zero FC (ZFC) magnetization of PFT at

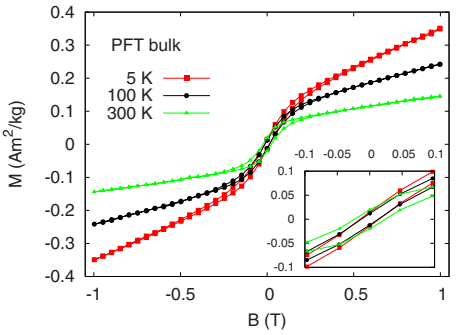

FIG. 9. (Color online) Magnetic hysteresis loop of $Pb(Fe_{1/2}Ta_{1/2})O_3$ at different temperatures. Inset shows magnification of hysteresis curve at low field.

different static applied fields [10 mT (not shown), 50 mT, 100 mT, 200 mT, 300 mT, 500 mT, and 1 T]. As can be seen, the magnetization is dependent on thermal history of the sample showing an irreversibility effect. A closer observation of magnetization reveals anomalies (slope change) at about 180(±5) K (T_{N1}) and 55(±5) K (T_{N2}) implying two possible magnetic transitions. The anomaly at about T_{N1} = 180 K agrees well with the known antiferromagnetic-PM (AFM-PM) transition in PFT single crystals.[2,15,32] However, the anomaly we observed at about 55 K (T_{N2}) could be related to the new magnetic transition. A possible existence of a new magnetic phase transition was suggested by Brixel *et al.*[33] at 9 K in PFT single crystal. The observed higher transition temperature for the new phase in the present case could be due to the presence of more disorder in our polycrystalline sample. Schmid[34] interpreted the new transition could be due to a weak long-range superexchange interaction between Fe-O-Ta-O-Fe, caused by short-range order at the *B* site. Recently, Lampis *et al.*[9] predicted the existence of two different Néel ordering temperatures by first-principles DFT calculations in the local spin density approximation and VASP.[9] This is explained in terms of two different superex-

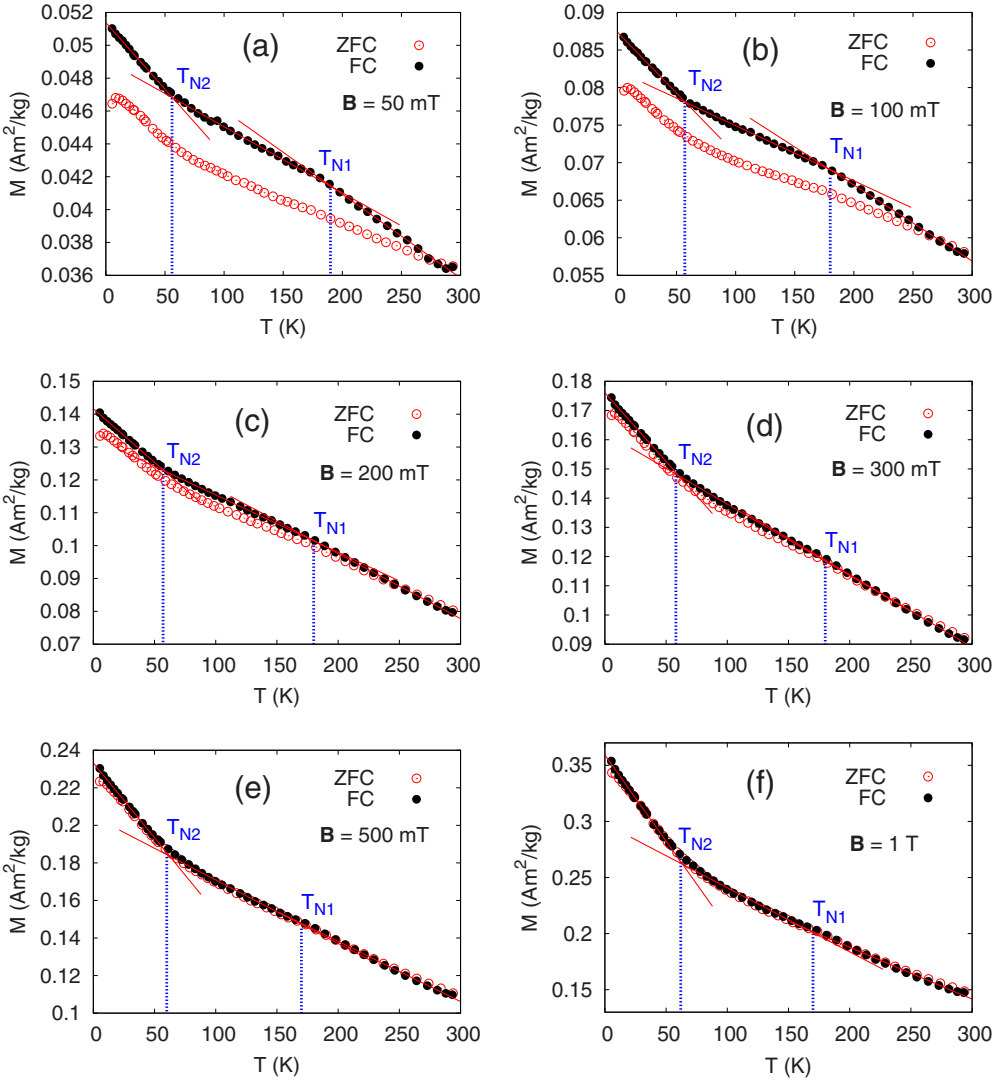

FIG. 10. (Color online) Temperature dependant of FC and ZFC Magnetization of $Pb(Fe_{1/2}Ta_{1/2})O_3$ at different constant static magnetic fields: (a) 50 mT; (b) 100 mT; (c) 200 mT; (d) 300 mT, (e) 500 mT, and (f) 1 T. T_{N1} represents Néel ordering temperatures from antiferromagnetic-paramagnetic transition whereas T_{N2} represents antiferromagnetic-antiferromagnetic transition with a possibly different spin orderings.

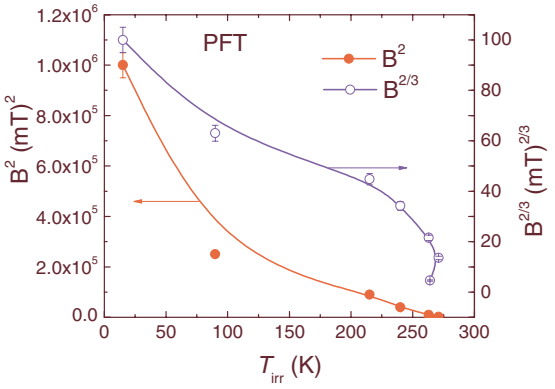

FIG. 11. (Color online) Field dependence of T_{irr} raised to the square and 2/3 powers for $Pb(Fe_{1/2}Ta_{1/2})O_3$. The data do not fit any critical lines (AT or GT) predicted for standard spin-glass materials. Note that the maximum and minimum of field are same for both the scales. The lines are guide to the eyes but not a fit. The expected evolution of T_{irr} as a function of field (square and power of 2/3) should be attributed to each model (presence of AT or GT critical lines).

change paths introduced by crystallographic ordering. Our observed low-temperature antiferromagnetic transition at T_{N2}=55 K (AFM-AFM transition with a possibly different spin orderings) agrees well with calculated value (48 K) by Lampis *et al.*[9]

The temperature at which irreversible magnetization, M_{irr} ($=M_{FC}-M_{ZFC}$) becomes nonzero called irreversibility temperature T_{irr}, where the ZFC and FC branches coalesce. The T_{irr} is shifting toward lower temperature with increasing field and ZFC and FC curves are almost superimposed at 1 T. The observation of shifting of T_{irr} with field is one of the salient features of spin-glasslike behavior.[35–38] ZFC magnetization shows a cusp at low temperature, which shifts toward lower temperature with applied field. This also supports the spin-glasslike behavior, as observed in PFT single crystal.[15]

In order to understand the frozen state and freezing transition, the behavior of magnetic field has been analyzed in the field-temperature (Fig. 11) plane ($T_{irr} \propto H^{2/3}$ and $T_{irr} \propto H^2$). As can be seen, the data neither follow the critical line predicted by de Almeida and Thouless (called AT line) for Ising spin glass, unlike that observed in single crystal below 30 K (Ref. 15) nor by Gabay and Toulouse (called GT line) for the Heisenberg spin glass.[35–38] This could be explained by the fact that our polycrystalline samples have more disorder compared to the single crystal. The exact nature of frozen disorder and magnetic frustration responsible for the spin-glasslike behavior is not yet well understood. However, our conjecture is that some of the paramagnetic spin clusters at Ta^{5+} site could have embedded into the ferromagnetic matrix at Fe^{3+} site because of equal ionic radii and short-range ordering of these ions due to charge difference (cf. Sec. III B) causing the randomness and magnetic frustration required for the origin of spin-glass behavior. Magnetic frustrations are usually caused by the competing interactions between ferromagnetic and antiferromagnetic orders. From Figs. 9 and 10 it is believed that there could be a ferromagnetic ordering in PFT. In order to understand the characteristic excitation of

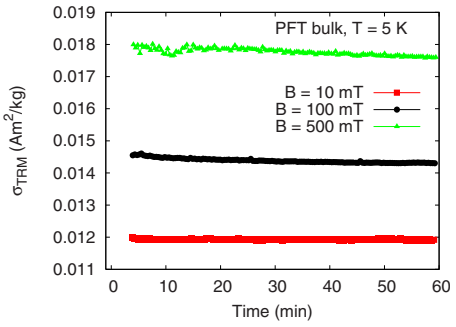

FIG. 12. (Color online) Time relaxation of thermoremanent magnetization (σ_{TRM}) of $Pb(Fe_{1/2}Ta_{1/2})O_3$ at 5 K with different fields.

spin glass and relaxation time, we investigated thermoremanent magnetization (σ_{TRM}) at 5 K with different fields (Fig. 12). To obtain the σ_{TRM}, the sample was field cooled from room temperature (i.e., above the T_{N1} and T_{N2}) and then the system was slowly cooled down in a constant field to 5 K (below T_{N1} and T_{N2}), at which the field was switched off and the time relaxation was followed. As can be seen from Fig. 12, the time relaxation is very slow, contrary to an exponential time decay observed in single crystal. An extremely slow relaxation of magnetization with time at low temperature is particularly an important and interesting characteristic signature of spin-glasses.[35–38] The observation of such slow relaxation suggest the possible presence of many metastable spin configurations. This type of slow relation was reported in other spin glass materials, i.e., $SrRuO_3$,[35] La_2CoMnO_6,[39] and AuFe alloy.[37,38]

G. Terahertz spectroscopy

The THz spectroscopy of polycrystalline PFT was measured in midinfrared (MIR) and far-infrared (FIR) ranges by using two spectrometers covering spectral band of 0.1–22 THz. A THz time-domain spectrometer was used to measure the transmission in the spectral region of 0.1–3 THz.[40] Figure 13(a) shows the measured time-domain waveform of reference and transmitted THz pulse at room temperature. The reference waveform was measured without sample in the THz path. The spectra obtained by performing Fourier transform of the waveforms are displayed in Fig. 13(b). The results show that the absorption of PFT in the range of 0.1–3 THz is so strong that almost no transmission signal was measured. Another separate experiment with Fourier transform infrared spectroscopy (Bruker IFS 66 V) was performed to measure the sample transmission in the range of 2 to 22 THz. The transmission spectra are shown in Fig. 13(c). As can be seen, almost no transmission was observed indicating that PFT is opaque in the region of MIR and FIR (0.1–22 THz).

IV. CONCLUSION

Polycrystalline samples of $Pb(Fe_{1/2}Ta_{1/2})O_3$ with a high percentage (97.3%) of perovskite phase were successfully synthesized by a solid-state reaction technique. EDS and SEM analyses showed nearly stoichiometric presence of all

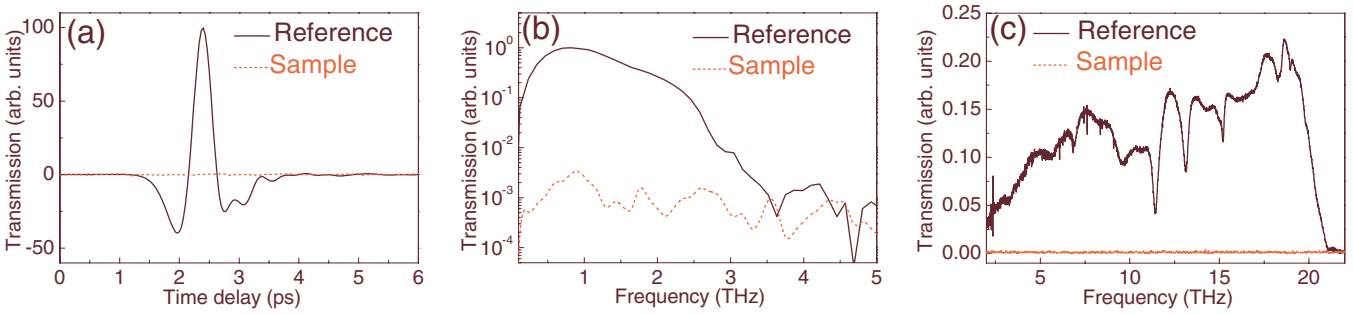

FIG. 13. (Color online) [(a) and (b)] THz spectra and (c) FTIR spectra of $Pb(Fe_{1/2}Ta_{1/2})O_3$ at room temperature.

the elements and uniform distributions of grain throughout the surface of the sample, respectively. XRD analysis showed that PFT possess an ideal cubic crystal structure with space group $Pm\bar{3}m$ at RT but the observation of forbidden Raman active modes in PFT reveals the existence of *hidden symmetry breaking*. The presence of several Raman active modes at RT provides an evidence of existence of nanoscale ordering in PFT. This observation answers the critical question, *"Is there a hidden symmetry breaking?"* asked by Geddo Lehmann *et al.*[5] with a *yes* answer.

PFT showed a multiferroic behavior (ferroelectric with magnetic ordering) at RT in the same phase. The temperature variation in field cooled magnetization showed the existence of two Néel temperatures (55 and 180 K) in agreement with theoretical predictions. The observation of spin-glasslike magnetic ordering at low temperature might have caused by antisite substitution of the Fe^{3+} and Ta^{5+} ions because of same ionic radii, however, more detailed study is needed to understand the exact nature of the randomness and magnetic frustration.

The dielectric response of the PFT showed a typical relaxor ferroelectric behavior with long-range disorder, which was evident from dielectric relaxation and a diffusive phase transition. PFT shows low dielectric loss and the loss is minimum at room temperature, which will be useful for practical applications. The current-voltage characteristics of PFT follows metal-insulator-metal capacitor behavior described by modified Simmons model. Magnetocapacitance and magnetoimpedance measurements show weak magnetoelectric coupling in PFT. It would be interesting to study thin films to enhance and control the magnetoelectric coupling for device applications. Dielectric measurements as a function of frequency showed a resonance at around 1.5 MHz with 180° phase angle change at high frequencies in agreement with theory. This phase change could be due to the presence of Ta in the sample. The ac conductivity measurements as function of temperature and frequency showed a thermally activated hopping conduction (extrinsic) at room temperature and high temperature whereas it has an ideal long-rang pathway conduction at low temperature. The ac conductivity has an excellent fit to the universal power law. THz measurements showed that the absorption of the PFT is very large in 0.1–22 THz. No transmission was observed implying an opaque nature of PFT in MIR and FIR range.

ACKNOWLEDGMENTS

The authors are thankful to Hans Schmid, University of Geneva and Seungbum Hong, Argonne National Laboratory for many helpful discussions. The authors would like to acknowledge financial support from DOE under Grant No. DE-FG02-08ER46526. We thank X.-C. Zhang, Rensselaer Polytechnic Institute for providing his THz facilities. R.P. thanks Institute of Functional Nanomaterial (IFN), UPR for financial support.

*r.palai@uprrp.edu

[1] G. A. Smolenskii, A. I. Agranovskya, and V. A. Isupov, Fiz. Tverd. Tela (Leningrad) **1**, 990 (1959) [Sov. Phys. Solid State **1**, 149 (1959)].

[2] S. Nomura, H. Takabayashi, and T. Nakagawa, Jpn. J. Appl. Phys. **7**, 600 (1968).

[3] W. Brixel, J. P. Rivera, and H. Schmid, Ferroelectrics **55**, 181 (1984).

[4] W. Brixel, R. Boutellier, and H. Schmid, J. Cryst. Growth **82**, 396 (1987).

[5] A. Geddo Lehmann, F. Kubel, Z.-G. Ye, and H. Schmid, Ferroelectrics **172**, 277 (1995).

[6] A. Geddo Lehmann, F. Kubel, and H. Schmid, J. Phys.: Condens. Matter **9**, 8201 (1997).

[7] A. Geddo Lehmann and P. Sciau, J. Phys.: Condens. Matter **11**, 1235 (1999).

[8] N. Lampis, P. Sciau, and A. Geddo Lehmann, J. Phys.: Condens. Matter **12**, 2367 (2000).

[9] N. Lampis, C. Franchini, G. Satta, A. Geddo-Lehmann, and S. Massidda, Phys. Rev. B **69**, 064412 (2004).

[10] H. Schmid, in *Crystal Growth*, edited by N. N. Sheftal (Consultants Bureau, New York, 1969) Vol. 7, 25

[11] J. Pastrnak and L. E. Cross, Phys. Status Solidi B **43**, K111 (1971).

[12] J.-F. Rossignol, J.-P. Rivera, and H. Schmid, Jpn. J. Appl. Phys., Part 1 **24**, 574 (1985).

[13] H. E. Muser, W. Kuhn, and J. Albers, Phys. Status Solidi A **49**, 51 (1978).

[14] K. Aso, J. Appl. Phys. **15**, 1243 (1976).
[15] A. Falqui, N. Lampis, A. Geddo-Lehmann, and G. Pinna, J. Phys. Chem. B **109**, 22967 (2005).
[16] R. Martinez, R. Palai, and R. S. Katiyar, *Mater. Res. Soc. Symp. Proc.* (Materials Research Society, Pittsburgh, 2008), Vol. 1034, p. 1034-K10-48.
[17] W. Z. Zhu, A. Kholkin, P. Q. Mantas, and J. L. Baptista, J. Eur. Ceram. Soc. **20**, 2029 (2000).
[18] R. N. P. Choudhary, R. Palai, and S. Sharma, Mater. Sci. Eng., B **77**, 235 (2000).
[19] http://abulafia.mt.ic.ac.uk/shannon/ptable.php
[20] R. P. Rosenstein and R. Schor, J. Chem. Phys. **38**, 1789 (1963).
[21] K. C. Kao, *Dielectric Phemomena in Solids* (Elsevier Academic Press, Amsterdam, 2004), p. 89.
[22] A. Moliton, *Applied Electromagnetism and Materials* (Springer, New York, 2007), p. 5.
[23] A. Moliton, *Applied Electromagnetism and Materials* (Springer, New York, 2007), p. 50.
[24] *Dielectrics Materials and Applications*, edited by A. R. Von Hippel (The Technology Press of M.I.T. and Wiley, New York, 1954), p. 24.
[25] A. Yellaiah, IEEE Conference on Electrical Insulator and Dielectric Phenonena, Annual Report (1993), p. 420.
[26] Q. Su, J. Zhou, K. M. Moulding, and D. J. Barber, Mater. Lett. **28**, 183 (1996).
[27] B.-C. Woo and B.-K. Kim, Jpn. J. Appl. Phys., Part 1 **42**, 6037 (2003).
[28] A. Vilan, J. Phys. Chem. C **111**, 4431 (2007).
[29] A. J. Moulson and J. M. Herbert, *Electroceramics*, 2nd ed. (Wiley, New York, 2003).
[30] A. K. Jonscher, J. Phys. D **32**, R57 (1999).
[31] J. C. Dyre and T. B. Schrder, Rev. Mod. Phys. **72**, 873 (2000).
[32] L. I. Shvorneva and Y. N. Venevtsev, Sov. Phys. JETP **22**, 722 (1966).
[33] W. Brixel, J.-P. Rivera, A. Steiner, and H. Schmid, Ferroelectrics **79**, 201 (1988).
[34] H. Schmid, Ferroelectrics **162**, 317 (1994).
[35] R. Palai, H. Huhtinen, J. F. Scott, and R. S. Katiyar, Phys. Rev. B **79**, 104413 (2009).
[36] M. Gruyters, Phys. Rev. Lett. **95**, 077204 (2005).
[37] K. Binder and A. P. Young, Rev. Mod. Phys. **58**, 801 (1986).
[38] K. H. Fischer and J. A. Hertz, *Spin Glasses* (Cambridge University Press, Cambridge, 1993).
[39] X. L. Wang, M. James, J. Horvat, and S. X. Dou, Supercond. Sci. Technol. **15**, 427 (2002).
[40] Q. Wu and X.-C. Zhang, Appl. Phys. Lett. **67**, 3523 (1996).